Metal/Metal-Oxide Interfaces: How Metal Contacts Affect the Work Function and Band Structure of MoO_3

Mark T. Greiner, Lily Chai, Michael G. Helander, Wing-Man Tang, and Zheng-Hong Lu*

When transition metal oxides are used in practical applications, such as organic electronics or heterogeneous catalysis, they often must be in contact with a metal. Metal contacts can affect an oxide's chemical and electronic properties within the first few nanometers of the contact, resulting in changes to an oxide's chemical reactivity, conductivity, and energy-level alignment properties. These effects can alter an oxide's ability to perform its intended function. Thus, the choice of contacting metal becomes an important design consideration when tailoring the properties of transition-metal oxide thin films or nanoparticles. Here, metal/metal-oxide interfaces involving a widely used oxide in organic electronics, MoO_3, are examined. It is demonstrated that metal contacts tend to reduce the Mo^{6+} cation to lower oxidation states and, consequently, alter MoO_3's valence electronic structure and work function when the oxide layer is very thin (less than 10 nm). MoO_3 becomes semimetallic and has a lower work function near metal contacts. The observed behavior is attributed to two causes: 1) charge transfer from the metal Fermi level into MoO_3's low-lying conduction band and 2) an oxidation-reduction reaction between the metal and MoO_3 that results in oxidation of the metal and reduction of MoO_3. These results illustrate how interfaces are important to an oxide's ability to provide energy-level alignment.

1. Introduction

Metal-oxide thin films are commonly used in organic electronic devices to enhance charge-transfer between electrodes and organic semiconductors. Oxides are coated onto electrodes, such as metals or transparent conductive oxides (TCOs), to improve the electrode's charge-injection characteristics. In the absence of a charge-injection buffer layer, metallic electrodes tend to have very high energy barriers for charge injection into organic semiconductors. With the incorporation a thin metal-oxide film, charge-injection can be made Ohmic. Numerous metal-oxides are used in organic electronic devices, some as hole-injectors (e.g., MoO_3, WO_3, V_2O_5, NiO, CuO),[1] and others as electron injectors (e.g., ZnO, ZrO_2, TiO_2).[2]

Dr. M. T. Greiner, L. Chai, Dr. M. G. Helander,
Dr. W. M. Tang, Prof. Z. H. Lu
Department of Materials Science and Engineering
University of Toronto
184 College Street, Toronto, Ontario, M5S 3E4, Canada
E-mail: mark.greiner@utoronto.ca

DOI: 10.1002/adfm.201200993

The low charge-injection barriers at metal-oxide/organic-semiconductor interfaces are believed to be a result of favourable energy-level alignment between metal-oxides and organic semiconducting molecules, which is largely influenced by the metal-oxide's work function.[3] As depicted in **Figure 1**, metal-oxide buffer layers in organic devices are generally between 1 and 10 nm thick, and are sandwiched between two interfaces: an interface with a solid organic semiconductor, and an interface with an electrode material. Most electrode materials are either metals or TCO's. Over the past 15 years, the organic electronics research community has thoroughly examined the metal-oxide/organic-semiconductor side of this multijunction,[4] yet relatively few papers have focused on the metal-oxide/electrode interface.[5,6]

Interfaces between metal-oxides and metals have been studied for many decades, especially in the fields of corrosion science, catalysis, and, more recently, inorganic semiconductor device research. However, within the context of organic electronics, the examination of metal-oxide/metal interfaces has only recently begun. Little is known regarding how metal-oxide/metal interfaces affect the oxide properties that are most relevant to organic electronic devices, namely work function and electron band structure.

When in contact with one another, oxides and metals can exhibit chemical and electronic interactions that affect their properties for several nanometers away from the metal/oxide interface. These interactions affect how nanostructured oxides perform in technological applications. For example, catalysis research has shown that oxides in thin-film form can possess enhanced catalytic activity compared to their bulk counterparts, due to charge-transfer interactions between the metal substrate and oxide on the nanometer length scale.[7] On the other hand, interfacial interactions can be detrimental to an application. For example, in inorganic-semiconductor applications, such as metal-oxide-semiconductor field-effect transistors (MOS-FETs), chemical reactions and defects at a metal/oxide interface can cause an oxide gate-dielectric to have high leakage current.[8]

In organic electronics devices, oxide layers are generally no more than a few nanometers thick. Minimal thickness is needed in order to decrease the series resistance oxides contribute to a device. As an oxide's properties can be affected for

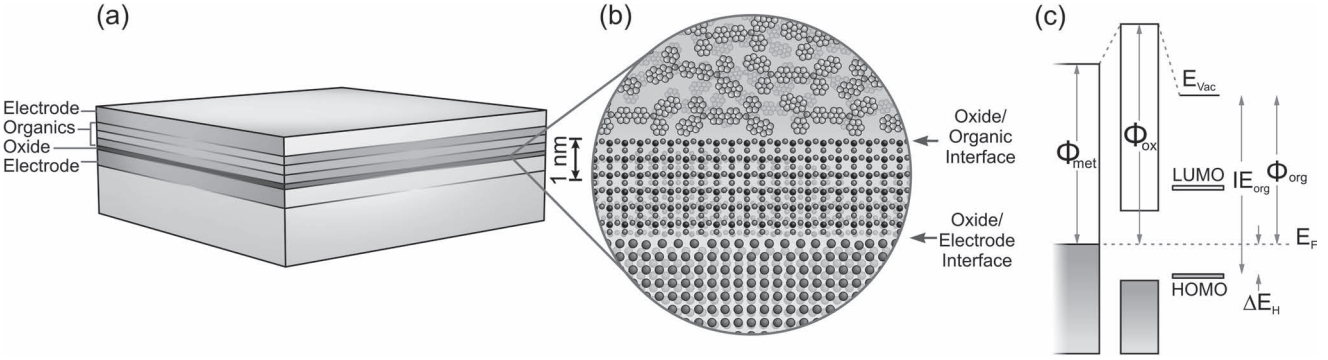

Figure 1. a) Illustration of a multilayered organic electronic device. b) Illustration of a metal-oxide buffer layer, demonstrating a typical thickness and highlighting the oxide/organic and oxide/electrode interfaces. c) Schematic energy-level diagram for a metal-oxide buffer layer.

several nanometers away from a metal interface, an oxide's ability to provide favourable energy-level alignment may be compromised by the near-by metal interface. Indeed, research has shown that energy-level alignment between an oxide and organic overlayers can change with oxide thickness.[5,9]

In the present paper, we demonstrate how various electrode interfaces can alter an oxide's work function and electronic band structure. We focus on an oxide that is commonly used as a hole-injection layer in organic devices, MoO_3. Over the past several years, the organic electronics community has thoroughly studied MoO_3.[5,6,9,10,11–13] MoO_3's very deep work function of ≈6.8–6.9 eV and its low-lying conduction band make it very useful as a hole-injection layer and p-type dopant in organic electronic devices.[12,13]

MoO_3 is a wide-band-gap semiconductor, with a band gap of ca. 3.0–3.1 eV.[5,13] It is a d^0 oxide, meaning the Mo 4d-band is considered empty, and its valence band is composed primarily of O 2p states.[14] A schematic energy-level diagram and valence band photoemission spectrum of MoO_3 is shown in **Figure 2**.

The electronic band structure of MoO_3 is highly dependent on the molybdenum cation oxidation state.[15] The dominant type of defect in MoO_3 is oxygen vacancies. Molybdenum cations in stoichiometric MoO_3 are Mo^{6+}, but oxygen vacancies cause Mo^{5+} cations to form, and result in a partially occupied Mo 4d-band within the MoO_3 band gap. These gap states act as n-type dopants and push MoO_3's Fermi level very close to the conduction band minimum.[13,15] As thermodynamics dictates that there is always some equilibrium concentration of defects, even "stoichiometric" MoO_3 is n-type. The gap state can clearly be seen in the valence-band photoemission spectra of oxygen deficient MoO_3, giving rise to a peak centered at ≈0.8 eV below the Fermi level, as shown in Figure 2b,c.

With continued removal of oxygen, MoO_3 can be reduced to the metallic oxide, MoO_2.[15,16] A schematic energy-band diagram and valence band photoemission spectrum of MoO_2 is shown in Figure 2. MoO_2, is the lowest stable molybdenum oxide, and it contains Mo^{4+} cations. The Mo^{4+} cations give rise to a partially filled d-band, resulting in an additional valence feature centered at ≈1.7 eV, as shown in Figure 2a. The gap state that was present in oxygen-deficient MoO_3 remains; however, it becomes broadened and actually crosses the Fermi level, making MoO_2 metallic.

In the present work, we show that metal contacts can cause MoO_3 to become semimetallic and have a decreased work function, as a result of molybdenum cation reduction at the metal/MoO_3 interface. These effects can persist for several nanometers

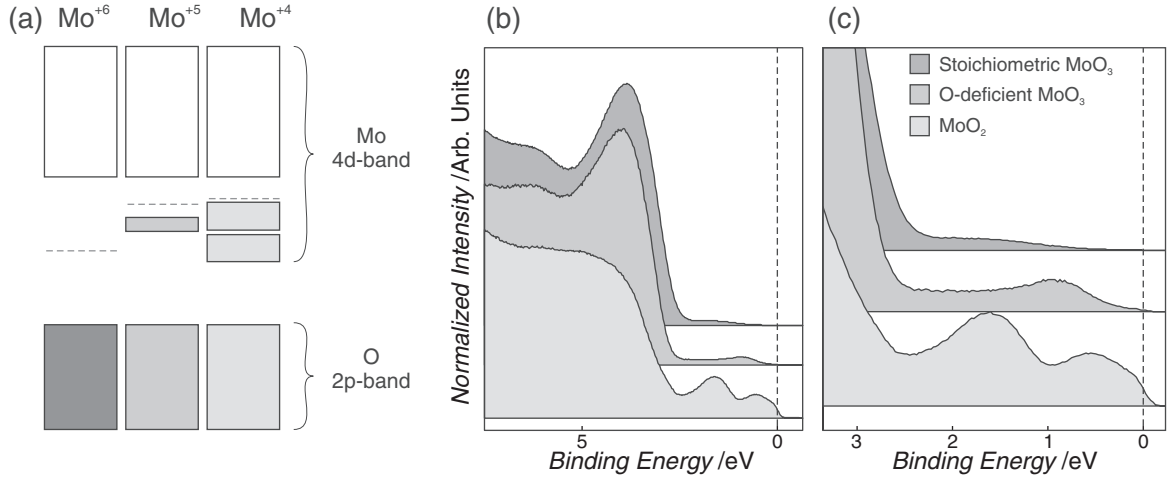

Figure 2. a) Schematic energy-level diagram of MoO_3, O-deficient MoO_3, and MoO_2. b) UPS valence band spectra and c) expanded view of the "defect" feature of MoO_3, O-deficient MoO_3 and MoO_2.

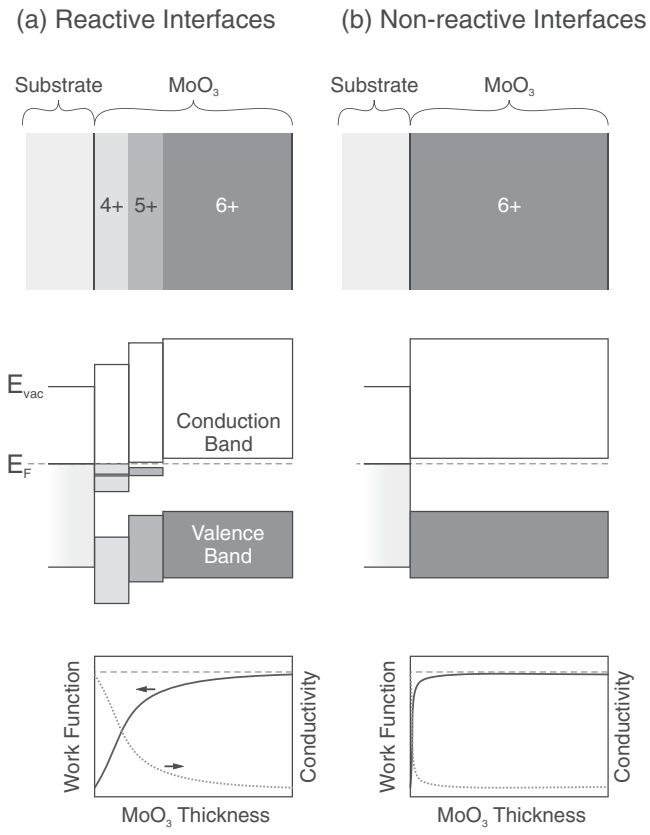

Figure 3. Schematic layered structure of MoO_3's oxidation states near an interface (top), schematic energy-band diagram for MoO_3 near an interface (middle), and plot of work function versus MoO_3 thickness and conductivity versus MoO_3 thickness (bottom) for reactive (a) and non-reactive (b) interfaces between MoO_3 and electrode materials.

away from the metal interface. Consequently, MoO_3's work function and electronic band structure exhibit thickness dependence. The degree of MoO_3 reduction and the distance from the interface, that MoO_3 is affected by the metal contact, is related to the metal's reactivity and work function. These interfacial interactions govern which thickness should be used when MoO_3 is paired with a particular electrode material, in order for to obtain an optimal balance of energy-level alignment and conductivity.

The metals examined here include a noble metal (Au), a high-work-function non-noble metal (Ni), the parent metal of MoO_3 (Mo), a reactive low-work-function metal (V), and an alloying metal (Cu). We find that the various metal/MoO_3 interfaces differ in terms of their reactivity. At highly reactive interfaces the Mo^{6+} cation of MoO_3 are reduced to Mo^{5+} and Mo^{4+} near the interface, while at less-reactive interfaces, MoO_3 is only slightly reduced. **Figure 3** illustrates the band structure profiles, work function profiles, and expected conductivity profiles of MoO_3 at reactive and non-reactive interfaces.

At reactive interfaces, the reduction of Mo^{6+} to Mo^{5+} and/or Mo^{4+} causes gap states to form in the MoO_3 band structure, which make the oxide more metallic or semimetallic near the electrode interface. With increasing distance from the interface, the oxide becomes more stoichiometric and insulating. Reduced cations also lower the oxide's work function near reactive interfaces. All of the metal/MoO_3 interfaces investigated here were found to be reactive; however, they differ from one another in terms of reactivity according to the following order: Au < Ni < Mo < Cu < V. While we did not observe any metals that formed non-reactive interfaces with MoO_3, non-reactive interfaces have been observed at metal-oxide/MoO_3 interfaces (such as CuO, NiO, V_2O_5, and ITO).

We propose that the factors that influence Mo^{6+} reduction at an interface are the oxygen potential and electron chemical potential (i.e., Fermi energy) of the substrate relative to MoO_3. A large difference in oxygen potential between MoO_3 and the substrate material can cause an oxidation/reduction reaction. A large difference in electron chemical potential can also cause Mo^{6+} cations to become reduced via charge-transfer with the substrate material.

2. Results

In stoichiometric MoO_3, molybdenum cations have a formal oxidation state of 6+. However, within the first few nanometers of each metal/MoO_3 interface the molybdenum cations of MoO_3 were found to be in a lower oxidation state, Mo^{5+} and/or Mo^{4+}. Note that molybdenum reduction may also be accompanied by oxygen loss, in which case the molecular formula should be written MoO_{3-x}; however, for simplicity we will continue to use the notation MoO_3 but we do not imply that the stoichiometry is strictly 1:3.

Interfacial reduction of Mo^{6+} to Mo^{5+} and/or Mo^{4+} is apparent from the XPS spectra. **Figure 4** shows the Mo 3d spectra of thin MoO_3 films grown on several metal substrates. In an oxide, Mo^{6+} appears at a binding energy of ≈232.5 eV, Mo^{5+} appears at ≈231.0 eV, Mo^{4+} at ≈229.5 eV and the Mo^0 of metallic molybdenum is at 228.0 eV. The precise binding energies of the oxidized molybdenum cations can vary by ±0.5 eV, depending on the oxide's Fermi level, which is influenced by the presence of defects and cation impurities.

The various metal substrates used here, differ from one another in terms of the amount of cation reduction they cause, as gauged by the average molybdenum oxidation state, determined from the relative peak areas in the XPS spectra of the thinnest MoO_3 films in Figure 4. The average oxidation state at each metal/MoO_3 interface is summarized in **Table 1**.

Molybdenum is found to be in its 6+ and 5+ oxidation states when MoO_3 is in contact with the metals Au, Mo, and Ni. While molybdenum is found to be in its 4+ and 5+ oxidation states when MoO_3 is in contact with V. Copper is a unique electrode metal in that it reacts with MoO_3 to form a Cu-Mo-O alloy.[17,18] The alloy contains both Mo^{6+} and Mo^{5+} species.

Based on the average molybdenum oxidation state detected at each interface, the degree of Mo^{6+} reduction increases in the following order: Au, Ni, Mo, V. This trend follows the trend of decreasing metal work functions: Au (5.3 eV), Ni (5.0 eV), Mo (4.5 eV), V (4.2 eV); however, it also follows the trend of decreasing metal oxidation potentials: Au→Au_2O_3 (appox. –9 kJ/mol), Ni→NiO (–419 kJ/mol), Mo→MoO_2 (–528 kJ/mol), V→VO (–800 kJ/mol).[19] Thus, the degree to which Mo^{6+} is

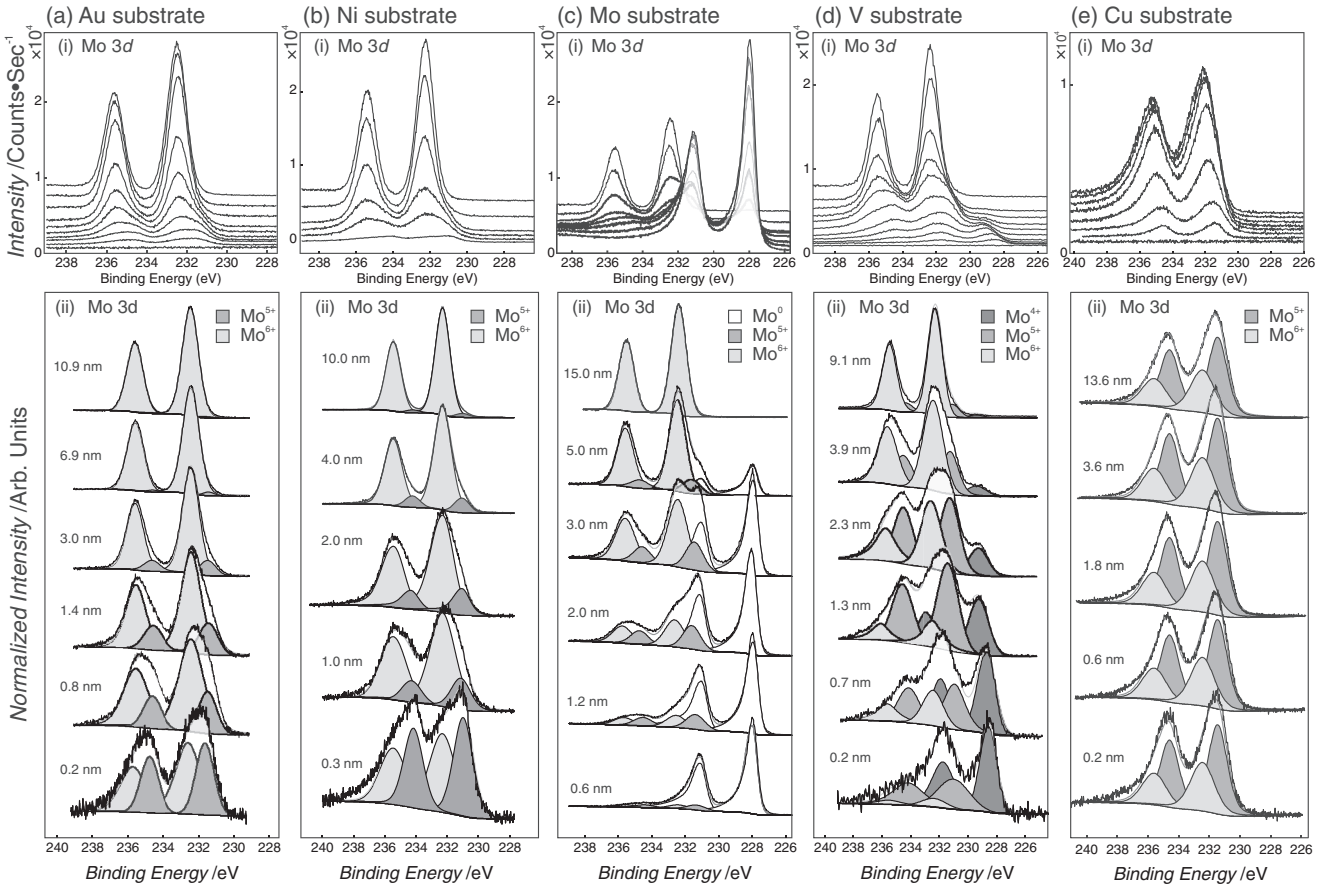

Figure 4. i) Mo 3d XPS spectra for MoO_3 films of various thicknesses deposited onto a) Au, b) Ni, c) Mo, d) V, and e) Cu substrates. ii) Peak fits of the spectra in (i) showing the component from Mo^{6+}, Mo^{5+} and Mo^{4+}.

reduced at a metal interface appears to depend on how easily electrons can be removed from the metal.

The average molybdenum oxidation state changes with MoO_3 thickness. Reduction of Mo^{6+} to lower oxidation states is only observed in close proximity to the metal/MoO_3 interface. Once the MoO_3 film is more than a few nanometers thick, only the Mo^{6+} cation can be detected by XPS. Note that this does not imply that, away from the interface, only Mo^{6+} cations are present in the MoO_3 film. Certainly Mo^{5+} cations are also present due to a non-zero concentration of O-vacancies. MoO_3 always contains O-vacancy defects at temperatures above 0 K, as a result of thermodynamic requirements. However, the O-vacancy concentration is too low for Mo^{5+} detection by photoemission.

Table 1. Summary of oxidation states present in MoO_3 films near the various metal interfaces.

Substrate Material	Average Mo Oxidation State	Mo^{6+}	Mo^{5+}	Mo^{4+}
Au	5.6	60%	40%	0%
Ni	5.5	50%	50%	0%
Mo	5.4	45%	55%	0%
V	4.5	7%	36%	57%
Cu	5.7	66%	34%	0%

MoO_3 work function increases with decreasing O-vacancy concentration.[15] The highest work function that could be obtained (i.e., for the most stoichiometric MoO_3) was 6.97 eV, regardless of whether the oxide was grown by Mo oxidation or by MoO_3 evaporation in vacuum. Note that the vapor phase over MoO_3 during sublimation consists of polymeric species with the formula Mo_xO_{3x}.[20] Thus, in bulk MoO_3 films deposited by sublimation, MoO_3 retains its 1:3 stoichiometry (with the exception of the small number of oxygen vacancies present due to entropy).

Oxidation-state profiles of each of the metal/MoO_3 interfaces are shown in **Figure 5**a. These profiles represent the relative Mo 3d peak areas for Mo^{6+}, Mo^{5+}, and Mo^{4+} peaks for each MoO_3 film thickness, as determined from the peak fitting shown in Figure 4. Note: due to the exponential dependence of XPS peak intensity with depth, and the fact that some films are thinner than the probing depth, these plots do not quantitatively represent the composition of the film at each given thickness. However, even after taking the depth sensitivity of XPS into account, the plots do indicate that there is a gradient in average oxidation state with distance from the metal interface. In contrast to the interfaces between MoO_3 and Au, Ni, Mo and V, Cu is

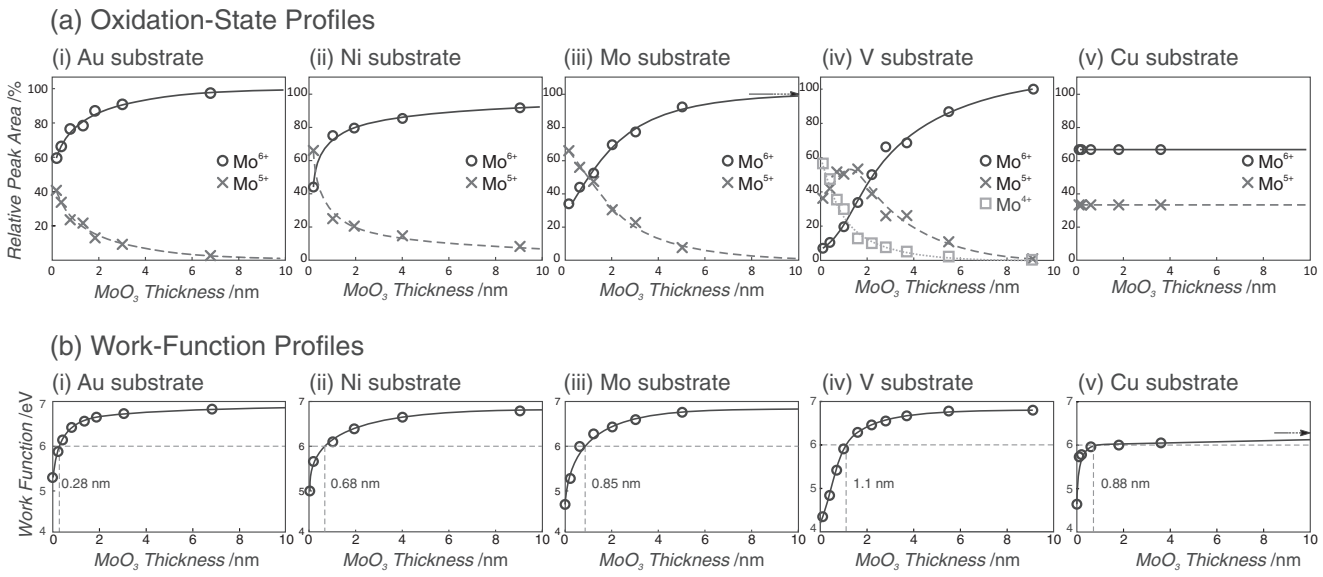

Figure 5. a) Oxidation state profiles and b) work function profiles for MoO_3 films grown on various metal substrates.

able to diffuse throughout the MoO_3 film, due to formation of a Cu-Mo-O alloy. Thus the oxidation state of Mo does not change with MoO_3 thickness, as shown in Figure 5a (v). The Cu-Mo-O alloy and its composition will be addressed further in the discussion section.

From the oxidation-state profiles in Figure 5a, one can see that the low-oxidation-state Mo cations persist further from the interface on the more reactive substrates than on the less-reactive substrates. As a figure-of-merit, we assign $d_{90\%}$ as the MoO_3 thickness for which Mo^{6+} peak is 90% of the total peak area. Then from Figure 5a we get $d_{90\%}$ values of 6.4 nm for V, 6.0 nm for Mo, 3.3 nm for Ni, and 2.8 nm for Au. Note that the Cu-Mo-O alloy never reaches 90% Mo^{6+}.

It was also found that work function depends on MoO_3 thickness. Work function tends to increase with distance away from the metal/MoO_3 interface, and eventually plateaus at a value of ~6.85–6.9 eV. Figure 5b shows plots of work-function versus MoO_3-thickness for each of the interfaces. The work-function profiles follow a similar trend to the cation-oxidation-state plots, suggesting that average cation oxidation state and work function are correlated. Note that the Cu-Mo-O alloy work function plateaus at ~6.25 eV.

Again we assign as a figure-of-merit, the thickness at which the work function reaches 6.0 eV, d_{6eV}. We get d_{6eV} values of 1.1 nm for V, 0.85 nm for Mo, 0.79 nm for Ni, and 0.28 nm for Au. Just as with the oxidation-state profiles, the MoO_3 work function reaches a high value closer to the interface with less-reactive metals. The fact that work function depends on MoO_3 thickness demonstrates why oxide thickness and substrate choice are important for energy-level alignment of molecular adsorbates. If a work function of greater than 6 eV is needed for Ohmic hole injection in an organic device, as is the case for common hole-transport materials such as CBP, then one must use a MoO_3 layer that is at least as thick d_{6eV}. Although the MoO_3 work function will decrease with time, due to adsorption of atmospheric contaminants,[11,21] in ultrahigh vacuum the rate of work function decrease is slow (ca. 0.15 eV decrease over 24 h, see Supporting Information). In device fabrication conditions (i.e., high vacuum), the rate of work function decrease is expected to be faster, but will also depend on the composition of the background gas (especially the carbon content).

Molybdenum cation reduction at the metal interfaces also causes significant changes to the MoO_3 valence band structure. **Figure 6**a,b show the UPS spectra taken for each MoO_3 thickness on each metal substrate. The MoO_3 thickness increases from top to bottom in the figure. Note: substrate reference spectra were subtracted from the spectra of the thinnest MoO_3 films to remove the substrate signal. The resulting spectra represent primarily the MoO_3 signal.

As MoO_3 is a d^0 oxide, the valence band maximum of stoichiometric MoO_3 is mainly composed of O 2p states. The O 2p band can clearly be distinguished in all UPS spectra, at binding energies ranging from about 5 eV to 3 eV. Note that for extremely thin MoO_3 films the O 2p band and higher-binding-energy features appear distorted by the interface. These distortions may be due to structural changes in the molybdenum-oxide lattice or due to changes in the substrate spectrum. The more significant features of the valence spectra are the additional states present in the band gap (between binding energies of 0 eV and 3 eV) that appear in the spectra close to the metal/MoO_3 interface. These gap states are observed at every metal/MoO_3 interface examined.

An enhanced view of the shallow valence regions is shown in Figure 6b. There are two distinct gap-state features, labelled d_1 and d_2. These states are known to arise in O-deficient d^0 oxides.[3,22] They arise due to electrons occupying the metal d-band.[23] When Mo^{6+} is reduced, excess electrons move into the low-lying Mo 4d orbitals, and give rise to donor states within the MoO_3 band gap, as illustrated in Figure 2. The d_1 feature resembles the feature that is found in MoO_3 when it has dilute O-vacancy defects, and the d_2 feature resembles the feature seen in MoO_3 when it has high O-vacancy defect concentrations and

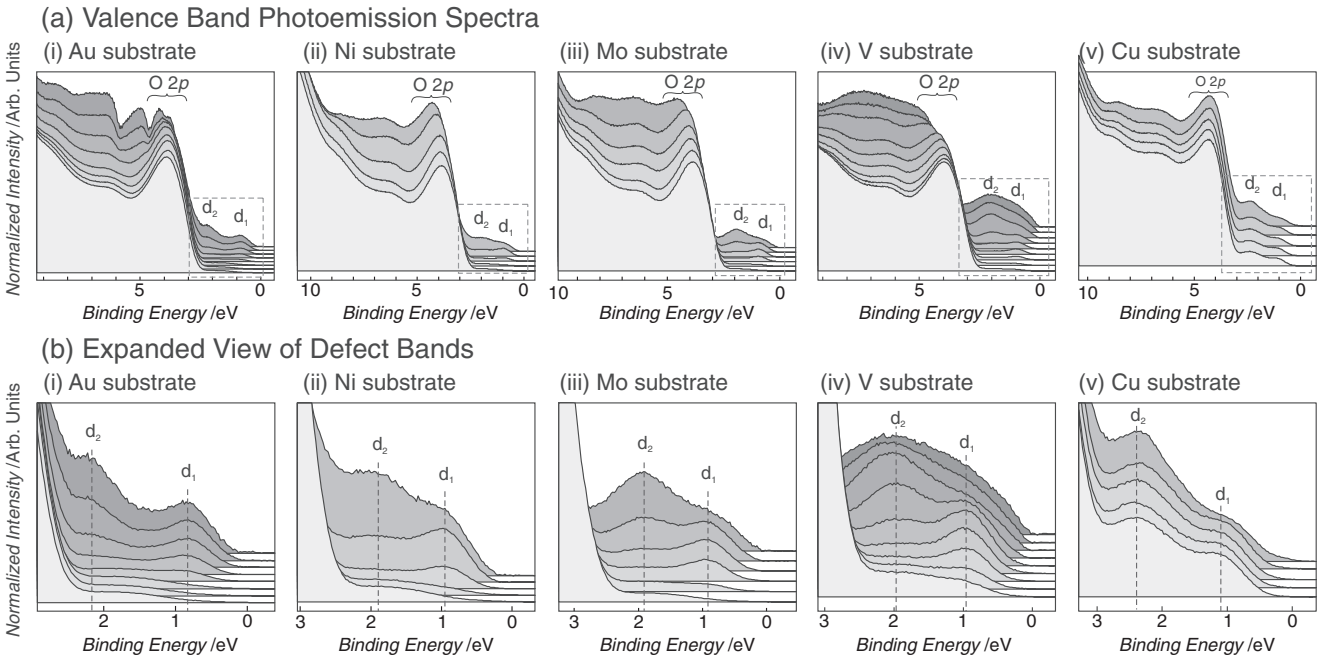

Figure 6. a) UPS valence band spectra and b) expanded view of the shallow valence features for MoO_3 films grown on various metal substrates. Gap states at the metal/MoO_3 interfaces are labelled d_1 and d_2.

is also seen in MoO_2 (compare with spectra shown in Figure 2). The intensities of the two defect features diminish as the MoO_3 film thickens, indicating that the oxide becomes less defective away from the interface. The higher-binding-energy feature, d_2, diminishes first, followed by the d_1 feature. Eventually, the valence spectrum of near-stoichiometric MoO_3 is obtained.

Due to the proximity of the observed gap states to the Fermi level, "MoO_3" would be expected to be metallic or semimetallic close to the metal interface. Note, we place MoO_3 in parentheses here because it is likely not stoichiometric, due to molybdenum reduction. Further away from the interface, where the gap states are no longer present, MoO_3 would be expected to have its typical bulk resistivity.

While the above observations indicate that MoO_3's properties are strongly affected by the metal interface, the metal's properties also may be affected by the interface. **Figure 7** shows XPS spectra of the metal substrate main peaks for clean substrate surfaces, spectra of substrates buried under ≈2 nm of MoO_3, and difference spectra (buried spectrum minus clean spectrum). One can see that the Au spectrum is not affected by the presence of MoO_3; however, Ni, Mo, and V show evidence of oxidation at the interface. The Cu spectra show that Cu is oxidized to Cu^+. Thus, the substrate spectra indicate that an oxidation-reduction reaction occurs for Ni, Mo, V and Cu, while there is no evidence of substrate oxidation in the case of Au.

3. Discussion

In the following sections we discuss the causes of reactivity at each interface in terms of oxidation thermodynamics and energy-level alignment. We address the importance of 1) substrate oxidation potential relative to overlayer oxidation potential and 2) substrate Fermi level relative to energy levels in MoO_3.

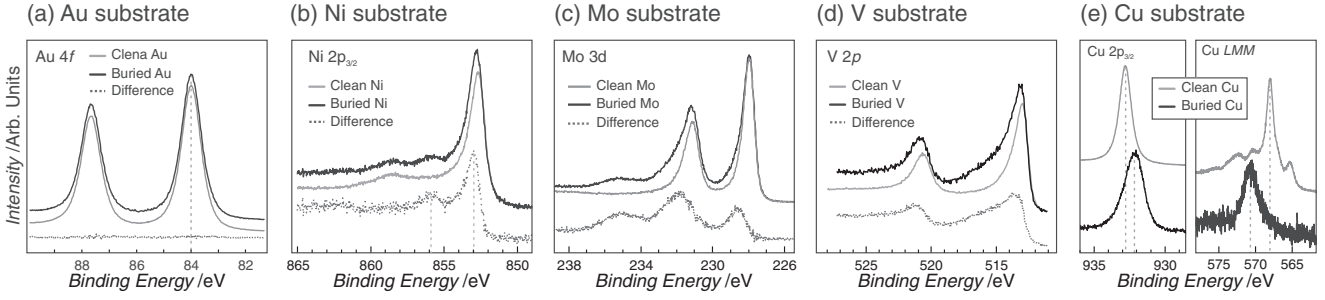

Figure 7. Core level XPS spectra of clean substrates and substrates buried under ≈2 nm of MoO_3. a) Au 4f, b) Ni $2p_{3/2}$, c) Mo 3d, d) V 2p, and e) Cu $2p_{3/2}$

3.1. Thermodynamic Considerations

One can predict whether a metal is capable of reducing an oxide using classical equilibrium thermodynamics. For example, consider two metals, $M^{(A)}$ and $M^{(B)}$, and their oxidation reaction:

$$M^{(A)} + \tfrac{1}{2}O_2 \rightarrow M^{(A)}O \qquad \Delta G^{(A)}_{O_2} = x \tag{1}$$

$$M^{(B)} + \tfrac{1}{2}O_2 \rightarrow M^{(B)}O \qquad \Delta G^{(B)}_{O_2} = y \tag{2}$$

By subtracting Equation (2) from Equation (1), we get the case where metal $M^{(A)}$ reduces the oxide $M^{(B)}O$:

$$M^{(A)} + M^{(B)}O \rightarrow M^{(A)}O + M^{(B)} \qquad \Delta G_{rxn} = x - y \tag{3}$$

Thus we can see that metal $M^{(A)}$ will spontaneously reduce oxide $M^{(B)}O$ if the free energy of oxidation for metal $M^{(A)}$ is more negative than the free energy of oxidation for metal $M^{(B)}$.

Values for free energy of oxidation for various metals can be determined from an Ellingham diagram. In **Table 2** we have compiled thermodynamic data for the reactions relevant to this work.[19] The reactions in Table 2 are ranked according to the free energy of oxidation for each reaction. The lower down on the table a reaction is, the more spontaneous it is. Thus VO is the most easily formed oxide and Au_2O_3 is the least easily formed one.

The thermodynamic data in Table 2 predicts whether a metal oxide is stable in the presence of another metal; however, it does not predict what concentration of defects will be stable at a metal/metal-oxide interface. In the case of MoO_3 we are interested in oxygen vacancy defects and cation oxidation-state defects. Oxygen vacancy defects affect an oxide's oxygen chemical potential, so one would expect that the oxygen vacancy concentration at the metal/MoO_3 interface would be such that the oxygen potential in defective MoO_3 equilibrates with the oxygen potential of the substrate metal.

Table 2. Thermodynamic data for selected metal oxidation reactions. All values except Au_2O_3 are from Reed[24] and are at 300 K. The values for Au_2O_3 are from.[25]

Label		Cation transition	Reaction equation	ΔG_{O2} (kJ•mol^{-1})
a	Au/Au_2O_3	$0 \rightarrow +3$	$4/3\ Au + O_2 \rightarrow 2/3\ Au_2O_3$	−2.3 to −8.7
b	VO_2/V_2O_5	$+4 \rightarrow +5$	$4VO_2 + O_2 \rightarrow 2V_2O_5$	−68.15
c	Cu_2O/CuO	$+1 \rightarrow +2$	$2Cu_2O + O_2 \rightarrow 4CuO$	−212.38
d	Cu/CuO	$0 \rightarrow +2$	$2Cu + O_2 \rightarrow 2CuO$	−253.12
e	MoO_2/MoO_3	$+4 \rightarrow +6$	$2MoO_2 + O_2 \rightarrow 2MoO_3$	−275.6
f	Cu/Cu_2O	$0 \rightarrow +1$	$4Cu + O_2 \rightarrow 2Cu_2O$	−293.87
g	V_2O_3/VO_2	$+3 \rightarrow +4$	$2V_2O_3 + O_2 \rightarrow 4VO_2$	−368.4
h	Ni/NiO	$0 \rightarrow +1$	$2Ni + O_2 \rightarrow 2NiO$	−419.37
i	Mo/MoO_3	$0 \rightarrow +6$	$2/3Mo + O_2 \rightarrow 2/3MoO_3$	−443.87
j	Mo/MoO_2	$0 \rightarrow +4$	$Mo + O_2 \rightarrow MoO_2$	−528
k	V/V_2O_5	$0 \rightarrow +5$	$4/5V + O_2 \rightarrow 2/5V_2O_5$	−539.87
l	In/In_2O_3	$0 \rightarrow +3$	$4/3In + O_2 \rightarrow 2/3In_2O_3$	−549.79
m	V/VO_2	$0 \rightarrow +4$	$V + O_2 \rightarrow VO_2$	−657.8
n	VO/V_2O_3	$+2 \rightarrow +3$	$4VO + O_2 \rightarrow 2V_2O_3$	−662
o	V/V_2O_3	$0 \rightarrow +3$	$4/3V + O_2 \rightarrow 2/3V_2O_3$	−754.25
p	V/VO	$0 \rightarrow +2$	$2V + O_2 \rightarrow 2VO$	−800.84

The chemical equation for oxygen vacancy formation is (using Kröger-Vink notation):

$$O^x_O + 2M^x_M = \upsilon^{\bullet\bullet}_O + 2M^{/}_M + \tfrac{1}{2}O_{2(g)} \tag{4}$$

Where O_Ox represents an oxygen atom on its regular lattice site, Mx_M represents a metal cation on its regular lattice site, $\upsilon^{\cdot\cdot}_O$ represents an oxygen vacancy with a charge of +2 relative to the neutral lattice, and $M^{/}_M$ represents a metal cation in a lower oxidation state than it has in the stoichiometric lattice. In the case of MoO_3, we can write:

$$O^x_O + 2Mo^{6+} = \upsilon^{\bullet\bullet}_O + 2Mo^{5+} + \tfrac{1}{2}O_{2(g)} \tag{5}$$

This equation shows that each oxygen vacancy gives rise to two reduced Mo cations. In the case of dilute defects, we can write the following equation relating Mo^{5+} cation concentration to the free-energy of formation of a vacancy (ΔG_{vO}):

$$\left[Mo^{5+}\right] = 2\left[\upsilon^{\bullet\bullet}_O\right] = 2^{1/3}\exp\left[\frac{-\Delta G_{\upsilon_O}}{3RT}\right]p^{-1/6}_{O_2} \tag{6}$$

Note that ΔG_{vO} represents the free energy of reaction (5), in which O_2 is the reaction product. It is also possible that oxygen abstraction can occur via some other reaction product, in which case the free energy of vacancy formation would be different. However, Equation (5) makes the free energy of vacancy formation comparable to the metal oxidation reactions in Table 1.

It is also useful to note bulk MoO_3 has three structurally distinct oxygen sites: asymmetric, symmetric and terminal sites.[26] Furthermore, oxygen vacancies most likely form from surface sites, and different surface sites are expected to have different vacancy formation energies. The vacancy formation energy experimentally measured from bulk MoO_3, and the value used in this work, likely represents the formation energy of the most labile oxygen site. Theoretical calculations have shown bridging oxygen to be the most labile oxygen site on the (010) surface.[27]

Equation (6) shows that, if a metal's oxygen potential (p_{O2}) is lower than that of "stoichiometric" MoO_3, then at the metal/MoO_3 interface, MoO_3 will have more O-vacancies than it has in its "stoichiometric" form. If the metal's p_{O2} is greater than that of "stoichiometric" MoO_3 then MoO_3 will have fewer O-vacancies at the interface than it has in its "stoichiometric" form.

One can estimate the enthalpy of formation for oxygen vacancies in MoO_3 using the heat of atomization of MoO_3 and an empirical relation proposed by Kofstad.[28] The relation is $\Delta H_v = 2(E_a - 167)$, where ΔH_v is the vacancy formation enthalpy in kcal/mol and E_a is the heat of atomization of the oxide in kcal/mol. This method of calculating vacancy formation energy yields a value that is related to the average M-O bond energy. This estimate results in a value of *ca.* 36 kJ/mol of oxygen vacancies in MoO_3.

3.2. MoO_3 on Au

According to the thermodynamic data in Table 2, such as reactions e and i, Au is not expected to reduce MoO_3 to either metallic Mo or MoO_2. Furthermore, as oxygen potentials

should equilibrate at a metal/metal-oxide interface, it is also not expected that the Au/Au_2O_3 reaction could cause any more oxygen vacancy defects to form in MoO_3 than are already present in "stoichiometric" MoO_3. In agreement with the conclusion that MoO_3 cannot oxidize Au, we see no evidence of chemical changes to Au at the buried interface, as shown in the Au 4f XPS spectra in Figure 7. The Au 4f spectrum exhibits no peak shift and no additional peaks in the buried spectrum.

Yet surprisingly we see from the XPS and UPS spectra in Figure 4 and 6 that Au causes Mo^{6+} to be reduced to Mo^{5+} within the first few nanometers of the Au/MoO_3 interface. While this is peculiar, it is not the first observation of this phenomenon. In fact there have been several reports of inert metals exhibiting charge-transfer with metal-oxides on the nano-scale, such as Au nanoparticles on MgO supports,[29] MgO films on Au surfaces,[30] thin WO_3 films on Pt surfaces,[31] MoO_3 films on Au surfaces,[32,33] Au nano-particles an TiO_2,[34] and V_2O_5 films on Au.[35] Although this phenomenon has been modeled computationally,[32,36] and lattice strain appears to be closely related to the charge-transfer process, this behaviour is still under debate.[37] Nonetheless, it appears that, even though classical thermodynamics does not predict it, in nanoscopic systems, charge transfer is possible between Au and various metal-oxides even though an interfacial chemical compound is not formed.

The Au/MoO_3 system has been examined before using photoemission spectroscopy (PES)[6,33] and scanning tunnelling microscopy (STM) supported with density-functional theory (DFT) calculations.[32] The PES study found evidence of Mo^{5+} at the interface, and it was suggested that electrons are donated to the Mo cations that have near-by oxygen vacancies. In the STM study, it was found that the MoO_3 lattice is strained at the interface. DFT calculations suggested that this strain allowed Au electron density to transfer to MoO_3. The DFT calculations also suggested that MoO_3 becomes semimetallic near the Au/MoO_3 interface. From Figure 6a-i and b-i we can see that indeed MoO_3 takes on a semimetallic MoO_2-like band structure at the Au/MoO_3 interface. This is due to partial filling of the Mo 4d band.

Our findings are consistent with the hypothesis of electron transfer from Au to Mo. But if Au transfers charge to Mo, without itself being oxidized, then what drives the charge-transfer process? MoO_3 is clearly reduced at the Au/MoO_3 interface. The XPS and UPS spectra do resemble oxygen-deficient MoO_3, but does this necessarily imply that Au has caused MoO_3 to become oxygen deficient? The law of mass action does not allow for excess oxygen vacancies in MoO_3 unless either Au forms and oxide or O_2 is released. There is no evidence of Au oxidation; however, it is possible that oxygen is lost as O_2 when MoO_3 condenses on the Au surface. The MoO_3 stoichiometry could not conclusively establish whether MoO_3 is oxygen deficient at the Au/MoO_3 interface, as XPS peak areas for such thin films could only determine the stoichiometry with a precision of no better than ±1%.

While O_2 removal may be possible, DFT calculations from Quek et al. suggest that electron transfer from Au to Mo is accompanied by a lattice distortion in MoO_3, while maintaining its stoichiometry.[32] So if the $Mo^{6+} \rightarrow Mo^{5+}$ reaction can occur without forming oxygen vacancies at all, what is the driving force? This reaction may be a result of gold's Fermi level being higher in energy than MoO_3's conduction band minimum. Thus an electron would come from the Au Fermi level, leaving a hole in the Au valence band, which stabilizes Mo^{5+} cations. One could therefore consider another defect reaction (again using Kröger-Vink notation):

$$e_{VB} + M_M^x = h_{VB}^{\bullet} + M_M^{/} \tag{7}$$

Where e_{VB} represents an electron at the metal Fermi level, M_Mx represents a metal cation in the oxide on its regular lattice site, $h^{\bullet}_{VB}$ represents a hole in the metal valence band, having a charge of +1 relative to the neutral metal, and $M^{/}_M$ is a reduced metal cation in the oxide. In the case of the Au/MoO_3 interface, one can write:

$$e_{(Au)} + Mo^{6+} \rightarrow h_{(Au)}^{\bullet} + Mo^{5+} \tag{8}$$

Where $e_{(Au)}$ represents an electron at the Au Fermi level, and $h^{\bullet}_{(Au)}$ represents a hole at the Au Fermi level. We then get the following equilibrium constant:

$$K = \frac{\left[h_{(Au)}^{\bullet}\right]\left[Mo^{5+}\right]}{\left[e_{(Au)}\right]\left[Mo^{6+}\right]} \tag{9}$$

As the denominator in this equation will be ≈1, and $[h^{\bullet}_{(Au)}] = [Mo^{5+}]$, one can write the following equation for $[Mo^{5+}]$:

$$\left[Mo^{5+}\right] = \left[h_{(Au)}^{\bullet}\right] = \exp\left[\frac{-\Delta G_f}{kT}\right] \tag{10}$$

Where ΔG_f is the energy needed to move an electron from the Au Fermi level to a Mo^{6+} site. One can approximate ΔG_f as the difference between the Au work function and the MoO_3 conduction band minimum, resulting in the following equation:

$$\left[Mo^{5+}\right] = \exp\left[\frac{-\left(\phi_{Au} - E\,A_{MoO_3}\right)}{kT}\right] \tag{11}$$

Figure 8 shows a schematic band diagram of the Au and MoO_3. The energy-level positions represent the valence bands,

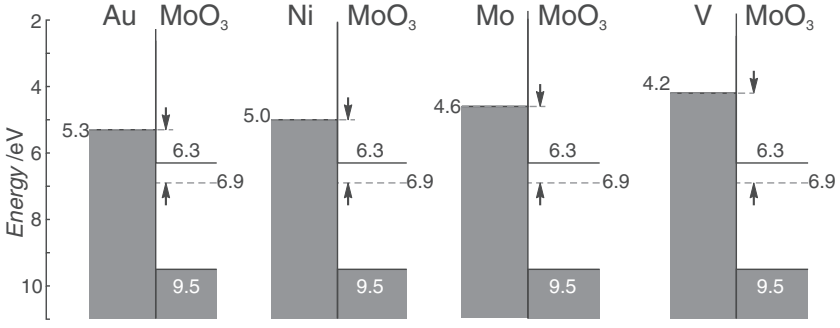

Figure 8. Schematic energy-band diagrams (vacuum-level alignment condition) for the metal/MoO_3 interfaces examined in this work. The shaded areas represent valence bands and white areas represent conduction bands. The dashed lines represent Fermi levels. The numbers represent valence band, conduction band, or Fermi level positions relative to the vacuum level.

conduction bands and Fermi levels of each material prior to contact. This analysis implies that Mo^{6+} is reduced to Mo^{5+} because of the position of Au's Fermi level relative to MoO_3's conduction band minimum, and that charge compensation is provided by the screening from the Au Fermi level, not by oxygen vacancies. Such charge compensation would not persist further away from the Au/MoO_3 interface. Indeed, the defect states in the valence spectrum become undetectable after about 2 nm of MoO_3 have been deposited. Likewise, the MoO_3 work function plateaus rather quickly.

Note that the reason why Au does not exhibit a peak shift is likely because any charge donated to MoO_3 is immediately replenished, as the Au sample is grounded. Au binding energy shifts have been observed previously when Au was present as nano-particles on an oxide support.[34,38] In these cases the Au particles become charged, but not oxidized or reduced.

3.3. MoO_3 on Ni

Nickel is similar to gold in that they are both high work function metals (Ni: $\phi = 5.0$ eV; Au: $\phi = 5.3$ eV). However, Ni can be oxidized much more easily than Au, with the formation enthalpy of NiO being ca. −419 kJ/mol, and the formation enthalpy of Au_2O_3 reported at ca. −3 to −9 kJ/mol.[25] Therefore, there is the possibility of not only electron transfer from Ni to MoO_3 from the Ni Fermi level, but also the possibility of Ni becoming oxidized by MoO_3, and subsequent removal of oxygen from MoO_3.

At room temperature, the free energy of the reaction: $2Ni + O_2 \rightarrow 2NiO$, is $\Delta G_{O2} = -419$ kJ/mol. While the free energy of the MoO_3 reduction reaction: $2MoO_3 \rightarrow 2MoO_2 + O_2$, is $\Delta G_{O2} = +275$ kJ/mol. Therefore, Ni can reduce MoO_3 according to the reaction: $Ni + MoO_3 \rightarrow MoO_2 + NiO$, $\Delta G = -72$ kJ/mol. Thus Ni oxidation provides a driving force for Mo^{6+} reduction that is in addition to electron transfer from the Ni Fermi level.

While Mo^{5+} is certainly evident in the Mo3d spectra, there is no detectible Mo^{4+}. Thus it appears that Ni does not completely reduce MoO_3 to MoO_2 at the interface, and perhaps only oxygen vacancies are formed. Complete reduction of MoO_2 may be possible at higher temperatures, where solid-state diffusion becomes more rapid.

In contrast to Au/MoO_3, the Ni $2p_{3/2}$ XPS spectrum shows evidence of Ni oxidation at the interface, as expected based on thermodynamic data. The Ni $2p_{3/2}$ XPS spectrum shown in Figure 7 compares a clean Ni surface with Ni buried under ca. 2 nm of MoO_3. By subtracting the clean Ni spectrum from the buried-interface spectrum, one can see that an additional peak is present at a binding energy of ca. 853.0 eV, as well as a possible satellite feature at *ca.* 856.0 eV.

3.4. MoO_3 on Mo

In the case of the Mo/MoO_3 interface, the metal substrate and the metal cation in the oxide are the same element, in contrast to the other interfaces examined in this work, where the cation in the oxide is a different element than the metal substrate. This is the same type of interface that is relevant to metal oxidation and corrosion. However, in the present case we have grown MoO_3 on Mo by evaporating MoO_3 rather than by oxidizing Mo, simply for direct comparison with the other samples. MoO_3 grown by Mo oxidation yields essentially the same results (see Supporting Information).

From corrosion studies it is known that, if a metal has more than one stable oxide, a layered oxide structure is possible. For example, when Fe is oxidized in dry oxygen, the structure of $Fe/FeO/Fe_3O_4/Fe_2O_3$ is obtained.[39] In this case, the layers are ordered according to increasing oxygen potential, from the metal outward. Layered structures can be predicted using metal-oxygen phase diagrams. If there is no boundary on the phase diagram showing equilibrium between an oxide and its metal, then that particular oxide will not equilibrate with the metal, and some lower-oxidation-state oxide must exist in between. Often, the intermediate oxides are non-stoichiometric, defective oxides.

Based on the Mo-O phase diagram, MoO_3 is not expected to equilibrate directly with Mo.[40] There are several intermediate, non-stoichiometric phases with mixed oxidation states that are stable in between MoO_3 and Mo. The oxide that equilibrates directly with Mo is MoO_2. Although we cannot discern a Mo^{4+} peak from the XPS spectra, we cannot eliminate the possibility that it exists, because the intense metal substrate obscures the ability to peak-fit the spectrum.

As molybdenum's Fermi level sit above MoO_3's conduction band minimum, as shown in Figure 8, we expect that the interfacial reduction of Mo^{6+} is a consequence of both molybdenum metal oxidation and charge transfer from the Mo Fermi level.

3.5. MoO_3 on V

Vanadium is the most reactive metal examined in this study. It very easily oxidizes, first to VO, then to V_2O_3, VO_2, and V_2O_5. Based on the thermodynamic data in Table 2, vanadium is expected to reduce MoO_3. In fact most of the vanadium oxides are expected to reduce MoO_3, according to the following reactions:

$$V + MoO_3 \rightarrow MoO_2 + VO \quad \Delta G = -262.6 \text{ kJ/mol}$$

$$2VO + MoO_3 \rightarrow MoO_2 + V_2O_3 \quad \Delta G = -193.2 \text{ kJ/mol}$$

$$V_2O_3 + MoO_3 \rightarrow MoO_2 + 2VO_2 \quad \Delta G = -46.4 \text{ kJ/mol}$$

Indeed, the photoemission spectra show severe MoO_3 reduction at the interface. The V/MoO_3 interface is the only one where significant amounts of Mo^{4+} are detected. In fact, very little Mo^{6+} is found at the interface.

The energy-level diagrams of V and MoO_3 also suggest that electrons can transfer from the V Fermi level to the MoO_3 conduction band, as shown in Figure 8. The severe MoO_3 reduction at the V/MoO_3 interface also causes major changes to MoO_3's band structure, causing its valence band to become similar to that of MoO_2. Based on the UPS spectra in Figure 6 iv, 'MoO_3' remains semimetallic even up to 6 nm from the V/MoO_3 interface. Note that the probing depth of UPS is extremely small (on the order of 1 Å), making these spectra very surface sensitive. Thus there is minimal contribution from buried layers.

3.6. MoO_3 on Cu

While Cu is a good electrode material due to its very low sheet resistance and its relatively low optical absorbance, the fact that Cu alloys with MoO_3 restricts MoO_3's ability as a buffer layer to provide energy-level alignment, because it cannot reach as high a work function as pure MoO_3 can. The maximum work function that the Cu-Mo-O alloy could achieve was ≈6.3 eV. This is likely due to the fact that the alloy always has a mix of Mo^{5+} and Mo^{6+} regardless of the oxide thickness; the low electronegativity of Mo^{5+} decreases the oxide's work function.

The Cu-Mo-O alloy that was formed has a rather interesting composition. The Mo 3d spectra (Figure 4 e) indicate that it contains Mo^{5+} and Mo^{6+}, with binding energies of ≈231.1 eV and 232.0 eV, respectively. The Cu $2p_{3/2}$ spectrum (Figure 7 e) gives a peak centered at ≈932.0 eV, which is indicative of Cu^+. However, as the Cu $2p_{3/2}$ peaks for Cu^0 and Cu^+ species are very close in proximity for copper oxides, we also examined the Cu *LMM* spectrum (Figure 7 e). This spectrum clearly shows a peak at 570.7 eV, which identifies the Cu species as Cu^+.[5]

On examining the UPS spectra (Figure 6 v), one finds that the valence band resembles that of MoO_3 except that the gap-state bands d_1 and d_2 are present. This valence structure suggests that when Cu is oxidized to Cu^+, it reduces Mo^{6+} to Mo^{5+}, donating electrons to the MoO_3 conduction band, resulting in a partially filled Mo 4d-band. The oxide retains its MoO_3-like structure. Thus, Cu acts similar to an n-type dopant in MoO_3. While the Cu-Mo-O alloy's band structure has the d_1 and d_2 gap states, similar to MoO_2, the valence band maximum of Cu-Mo-O does not cross the Fermi level, but sits ≈0.4 eV below it.

Based on XPS peak areas, the oxide alloy has an atomic composition of ≈71.4% O, 3.5% Cu and 25.1% Mo. From these numbers, it appears that Cu^+ displaces O^{2-}. But if one Cu^+ displaces one O^{2-}, then the lattice becomes charged +3 relative to the neutral MoO_3 lattice. This would require three $Mo^{6+} \rightarrow Mo^{5+}$ reductions. Therefore, we propose the following general formula: $Cu_xMo^{(VI)}_{y-3x}Mo^{(v)}_{3x}O_{3y-x}$. Using the atomic compositions determined from XPS peak areas, we arrive at a formula of $Cu_1Mo^{(VI)}_2Mo^{(V)}_3O_{14}$. This composition is similar to composition ranges reported previously for Cu-Mo-O alloys.[17,41]

Although this compound does not have as high a work function as stoichiometric MoO_3, its work function is still reasonably high and it could still be used as an anode material for many hole-transporting organic semiconductors. It also has a high density of states close to the Fermi level, which may make it more conductive than stoichiometric MoO_3.

3.7. Work Function and Cation Oxidation State

While molybdenum oxidation state follows a gradient with MoO_3 thickness, we have also pointed out in Figure 5b that work function also changes with MoO_3 thickness. The fact that average Mo oxidation state and work function follow similar trends with MoO_3 thickness suggests that an oxide's work function is related to cation oxidation state in a rather simple way, i.e., that lower cation oxidation state results in lower work function. This has been proposed before,[42] and recently shown experimentally for several transition metal oxides.[15] The cause of the relationship is believed to be due to the fact that lower-oxidation-state cations are less electronegative than higher-oxidation-state ones, and electronegativity directly affects a solid's Fermi energy.

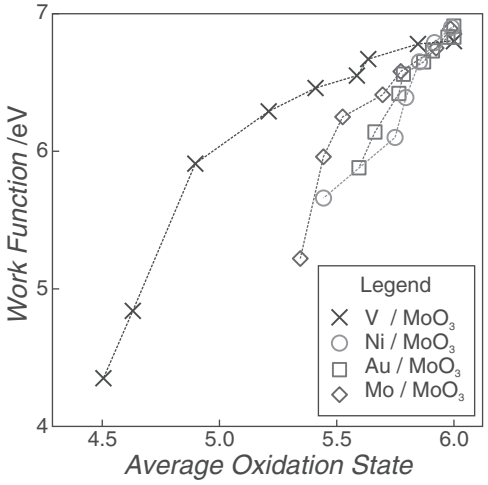

Figure 9. Plot of work function versus average Mo oxidation state in MoO_3 for MoO_3 films grown on various metal substrates.

Figure 9 shows plots of average molybdenum cation oxidation state, versus measured work functions for the metal/MoO_3 interfaces examined in this study. This figure illustrates that a positive correlation between cation oxidation state and work function. Thus, due to the presence of lower oxidation state cations near the metal/MoO_3 interfaces, MoO_3's work function is decrease within the first few nanometers of the interface. This behaviour affects how thick of an oxide one should use in an organic device in order to achieve optimal energy-level alignment. These effects may also alter the catalytic properties of metal oxide nanoparticles on metal supports, since ultra-high work function metal oxides would be needed to enable oxidation of molecules that have very large ionization energies.

4. Summary

We have examined several metal/MoO_3 interfaces using photoemission measurements of layer-by-layer grown MoO_3 films. We examined several metals (Au, Ni, Mo, V and Cu), which differ from one another in their work functions and their oxidation potentials. We find that when MoO_3 is grown on any of these metal substrates, Mo^{6+} cations are reduced to lower oxidation states (Mo^{5+} and Mo^{4+}) close to the metal/MoO_3 interface. The degree of Mo^{6+} reduction differs for each metal. We explain the interfacial MoO_3 reduction with two proposed mechanisms: 1) charge transfer from the metal Fermi level to the oxide conduction band, and 2) reduction of MoO_3 driven by oxidation of the metal substrate. With these mechanisms, we can explain why a noble metal, such as Au can reduce Mo^{6+} within the first few nanometers of the Au/MoO_3 interface, and why a reactive metal, such as V can cause severe reduction of Mo^{6+} for several nanometers from the interface.

We have also found that the interfacial reduction of Mo^{6+} results in changes to the MoO_3 valence band structure, making

the oxide semimetallic close to the metal interface. The valence band changes are explained in terms of electrons filling the previously empty Mo 4d states of MoO_3, resulting in donor states close to the Fermi level.

The presence of reduced molybdenum cations also results in a lower work function for MoO_3 close to the metal/MoO_3 interface. The work function increases as the average cation oxidation state increases. This implies that more reactive interfaces will require thicker oxide buffer layers before the maximum work function is achieved; however, more reactive interfaces will also be more conductive near the interface. This finding has implications to organic electronic device design and choosing the right oxide buffer thickness for the optimal balance of work function and conductivity.

5. Experimental Section

Photoemission spectra were collected using a Physical Electronics 5500 Multi-Technique system, using monochromated Al Kα radiation ($h\nu$ = 1486.7 eV) for XPS spectra and non-monochromated He Iα radiation ($h\nu$ = 21.22 eV) for UPS spectra and work function measurements. XPS spectra were collected using a take-off angle of 75°. UPS spectra and work function measurements were measured at a take-off angle of 88°. During UPS and work function measurements, the sample was held at a negative bias of –15 V relative to the spectrometer.

All MoO_3 films were grown by vacuum sublimation. 99.99% pure MoO_3 powder was placed into 10 cc cone-shaped alumina crucibles and placed in a Knudsen cell. MoO_3 was evaporated at a temperature of 550°C to obtain a deposition rate of ≈0.2 Å/s at the sample surface, as determined using an oscillating quartz thickness monitor. The samples were ≈1 cm × 1 cm. The evaporation source was positioned 31 cm away from the sample, at an angle of 35° (K-cell axis relative to sample normal). The pressure during deposition was $\approx 5 \times 10^{-9}$ torr.

Metal substrates were prepared by magnetron sputter deposition from 99.99+% pure metal targets onto epi-polished, degenerately p-doped Si substrates. Metal films were ≈200 nm thick. All metal films were sputter cleaned in the XPS chamber to remove atmospheric contamination and native oxide films prior to MoO_3 deposition.

Supporting Information

Supporting Information is available from the Wiley Online Library or from the author.

Acknowledgements

The authors gratefully acknowledge the financial support of the National Science and Engineering Research Council of Canada.

Received: April 8, 2012
Revised: July 25, 2012
Published online: August 17, 2012

[1] a) C. W. Chu, S. H. Li, C. W. Chen, V. Shrotriya, Y. Yang, *Appl. Phys. Lett.* **2005**, *87*, 193508; b) J. Z. Li, M. Yahiro, K. Ishida, H. Yamada, K. Matsushige, *Synth. Met.* **2005**, *151*, 141; c) H. You, Y. F. Dai, Z. Q. Zhang, D. G. Ma, *J. Appl. Phys.* **2007**, *101*, 026105; d) I. M. Chan, T. Y. Hsu, F. C. Hong, *Appl. Phys. Lett.* **2002**, *81*, 1899; e) G. B. Murdoch, M. Greiner, M. G. Helander, Z. B. Wang, Z. H. Lu, *Appl. Phys. Lett.* **2008**, *93*, 083309.

[2] a) H. J. Bolink, E. Coronado, D. Repetto, M. Sessolo, *Appl. Phys. Lett.* **2007**, *91*, 223501; b) N. Tokmoldin, N. Griffiths, D. D. C. Bradley, S. A. Haque, *Adv. Mater.* **2009**, *21*, 3475; c) H. J. Bolink, E. Coronado, D. Repetto, M. Sessolo, E. M. Barea, J. Bisquert, G. Garcia-Belmonte, J. Prochazka, L. Kavan, *Adv. Funct. Mater.* **2008**, *18*, 145.

[3] M. T. Greiner, M. G. Helander, W. M. Tang, Z. B. Wang, J. Qiu, Z. H. Lu, *Nat. Mater.* **2012**, *11*, 76.

[4] a) H. Ishii, K. Sugiyama, E. Ito, K. Seki, *Adv. Mater.* **1999**, *11*, 605; b) C. Tengstedt, W. Osikowicz, W. R. Salaneck, I. D. Parker, C. H. Hsu, M. Fahlman, *Appl. Phys. Lett.* **2006**, *88*, 053502; c) S. Braun, W. R. Salaneck, M. Fahlman, *Adv. Mater.* **2009**, *21*, 1450; d) H. Vazquez, W. Gao, F. Flores, A. Kahn, *Phys. Rev. B* **2005**, *71*, 041306.

[5] K. Kanai, K. Koizumi, S. Ouchi, Y. Tsukamoto, K. Sakanoue, Y. Ouchi, K. Seki, *Org. Elect.* **2010**, *11*, 188.

[6] Y. Yi, P. E. Jeon, H. Lee, K. Han, H. S. Kim, K. Jeong, S. W. Cho, *J. Chem. Phys.* **2009**, 130.

[7] a) M. Sterrer, T. Risse, U. M. Pozzoni, L. Giordano, M. Heyde, H.-P. Rust, G. Pacchioni, H.-J. Freund, *Phys. Rev. Lett.* **2007**, *98*, 096107; b) F. P. Netzer, F. Allegretti, S. Surnev, *J. Vac. Sci. Technol. B* **2010**, *28*, 1.

[8] G. D. Wilk, R. M. Wallace, J. M. Anthony, *J. Appl. Phys.* **2001**, *89*, 5243.

[9] Irfan, H. J. Ding, Y. L. Gao, D. Y. Kim, J. Subbiah, F. So, *Appl. Phys. Lett.* **2010**, *96*, 073304.

[10] a) T. Matsushima, Y. Kinoshita, H. Murata, *Appl. Phys. Lett.* **2007**, *91*, 253504; b) J. Meyer, R. Khalandovsky, P. Gorrn, A. Kahn, *Adv. Mater.* **2011**, *23*, 70; c) K. S. Yook, J. Y. Lee, *Synth. Met.* **2009**, *159*, 69; d) T. Matsushima, G. H. Jin, H. Murata, *J. Appl. Phys.* **2008**, *104*, 054501; e) H. Lee, S. W. Cho, K. Han, P. E. Jeon, C. N. Whang, K. Jeong, K. Cho, Y. Yi, *Appl. Phys. Lett.* **2008**, *93*, 043308; f) Y. Nakayama, K. Morii, Y. Suzuki, H. Machida, S. Kera, N. Ueno, H. Kitagawa, Y. Noguchi, H. Ishii, *Adv. Funct. Mater.* **2009**, *19*, 3746; g) M. Kröger, S. Hamwi, J. Meyer, T. Riedl, W. Kowalsky, A. Kahn, *Org. Electron.* **2009**, *10*, 932; h) S. Hamwi, J. Meyer, M. Kröger, T. Winkler, M. Witte, T. Riedl, A. Kahn, W. Kowalsky, *Adv. Funct. Mater.* **2010**, *20*, 1762.

[11] Irfan, H. Ding, Y. Gao, C. Small, D. Y. Kim, J. Subbiah, F. So, *Appl. Phys. Lett.* **2010**, *96*, 243307.

[12] a) T. Matsushima, G.-H. Jin, Y. Kanai, T. Yokota, S. Kitada, T. Kishi, H. Murata, *Org. Electron.* **2011**, *12*, 520; b) S. Hamwi, J. Meyer, T. Winkler, T. Riedl, W. Kowalsky, *Appl. Phys. Lett.* **2009**, *94*, 253307.

[13] M. Kröger, S. Hamwi, J. Meyer, T. Riedl, W. Kowalsky, A. Kahn, *Appl. Phys. Lett.* **2009**, *95*, 123301.

[14] D. O. Scanlon, G. W. Watson, D. J. Payne, G. R. Atkinson, R. G. Egdell, D. S. L. Law , *J. Phys. Chem. C* **2010**, *114*, 4636.

[15] M. T. Greiner, L. Chai, M. G. Helander, W. M. Tang, Z. H. Lu, *Adv. Funct. Mater.* **2012**, 10.1002/adfm.201200615.

[16] M. T. Greiner, M. G. Helander, Z. B. Wang, W. M. Tang, J. Qiu, Z. H. Lu, *Appl. Phys. Lett.* **2010**, *96*, 213302.

[17] a) T. E. Warner, E. M. Skou, *Mater. Res. Bull.* **2010**, *45*, 1635; b) U. Steiner, T. Morgenstern, W. Reichelt, H. Borrmann, A. Simon, *Z. Anorg. Allg. Chem.* **1994**, *620*, 1905.

[18] a) J. Haber, T. Machej, L. Ungier, J. Ziolkowski, *J. Solid State Chem.* **1978**, *25*, 207; b) R. S. Iordanova, M. K. Milanova, K. L. Kostov, *Phys. Chem. Glasses-Eur. J. Glass Sci. Technol. B* **2006**, *47*, 631.

[19] T. Reed, *Free Energy of Formation of Binary Compounds*, The MIT Press, Cambridge, MA **1972**.

[20] J. Berkowitz, M. G. Inghram, W. A. Chupka, *J. Chem. Phys.* **1957**, *26*, 842.

[21] a) I. Irfan, Y. Gao, *J. Photonics Energy* **2012**, *2*, 021213; b) J. Meyer, A. Shu, M. Kröger, A. Kahn, *Appl. Phys. Lett.* **2010**, *96*, 133308; c) C. H. Cheung, W. J. Song, S. K. So, *Org. Electron.* **2010**, *11*, 89; d) M. T. Greiner, M. G. Helander, Z.-B. Wang, W.-M. Tang, Z.-H. Lu, *J. Phys. Chem. C* **2010**, *114*, 19777.

[22] a) V. E. Henrich, P. A. Cox, *The Surface Science of Metal Oxides*, Cambridge University Press, Cambridge **1996**;b) L. E. Firment, A. Ferretti, *Surf. Sci.* **1983**, *129*, 155.
[23] V. E. Henrich, P. A. Cox, *The Surface Science of Metal Oxides*, Cambridge University Press, Cambridge **1994**.
[24] C. M. McShane, K. S. Choi, *J. Am. Chem. Soc.* **2009**, *131*, 2561.
[25] H. Q. Shi, R. Asahi, C. Stampfl, *Phys. Rev. B* **2007**, *75*, 205125.
[26] R. Coquet, D. J. Willock, *Phys. Chem. Chem. Phys.* **2005**, *7*, 3819.
[27] R. Tokarz-Sobieraj, K. Hermann, M. Witko, A. Blume, G. Mestl, R. Schlögl, *Surf. Sci.* **2001**, *489*, 107.
[28] P. Kofstad, *J. Phys. Chem. Solids* **1967**, *28*, 1842.
[29] P. Torelli, L. Giordano, S. Benedetti, P. Luches, E. Annese, S. Valeri, G. Pacchioni, *J. Phys. Chem. C* **2009**, *113*, 19957.
[30] Y. Pan, S. Benedetti, N. Nilius, H. J. Freund, *Phys. Rev. B* **2011**, *84*, 075456.
[31] Z. Li, Z. Zhang, Y. K. Kim, R. S. Smith, F. Netzer, B. D. Kay, R. Rousseau, Z. Dohnalek, *J. Phys. Chem. C* **2011**, *115*, 5773.
[32] S. Y. Quek, M. M. Biener, J. Biener, C. M. Friend, E. Kaxiras, *Surf. Sci.* **2005**, *577*, L71.
[33] Z. Song, T. H. Cai, Z. P. Chang, G. Liu, J. A. Rodriguez, J. Hrbek, *J. Am. Chem. Soc.* **2003**, *125*, 8059.
[34] K. Mitsuhara, Y. Kitsudo, H. Matsumoto, A. Visikovskiy, M. Takizawa, T. Nishimura, T. Akita, Y. Kido, *Surf. Sci.* **2010**, *604*, 548.
[35] S. Guimond, D. Gobke, Y. Romanyshyn, J. M. Sturm, M. Naschitzki, H. Kuhlenbeck, H. J. Freund, *J. Phys. Chem. C* **2008**, *112*, 12363.
[36] L. Giordano, G. Pacchioni, *Acc. Chem. Res.* **2011**, *44*, 1244.
[37] H. J. Freund, *Surf. Sci.* **2007**, *601*, 1438.
[38] Z. Q. Jiang, W. H. Zhang, L. Jin, X. Yang, F. Q. Xu, J. F. Zhu, W. X. Huang, *J. Phys. Chem. C* **2007**, *111*, 12434.
[39] R. M. Cornell, U. Schwertmann, *The Iron Oxides*, Wiley-VCH, Weinheim **2003**.
[40] L. Brewer, Lamoreaux, R.H., *Bull. Alloy Phase Diagrams* **1980**, *1*, 85.
[41] U. Steiner, W. Reichelt, H. Oppermann, *Z. Anorg. Allg. Chem.* **1996**, *622*, 1428.
[42] G. Campet, J. Portier, M. A. Subramanian, *Mater. Lett.* **2004**, *58*, 437.